AGU PUBLICATIONS

Paleoceanography and Paleoclimatology

RESEARCH ARTICLE
10.1002/2017PA003294

**Key Points:**
- Detailed speleothem-based ASM variability across HS 5 through 2
- Contrasting patterns of HS (rapid onset) and Bond events (gradual onset)
- Insights into dynamics of abrupt climate changes under different boundaries

**Supporting Information:**
- Supporting Information S1

**Correspondence to:**
D. Liu,
ldb9921@njnu.edu.cn

**Citation:**
Liu, D., Wang, Y., Cheng, H., Edwards, R. L., Kong, X., Chen, S., & Liu, S. (2018). Contrasting patterns in abrupt Asian summer monsoon changes in the last glacial period and the Holocene. *Paleoceanography and Paleoclimatology*, *33*, 214–226. https://doi.org/10.1002/2017PA003294

Received 21 NOV 2017
Accepted 20 DEC 2017
Accepted article online 4 JAN 2018
Published online 24 FEB 2018



# Contrasting Patterns in Abrupt Asian Summer Monsoon Changes in the Last Glacial Period and the Holocene

**Dianbing Liu[1], Yongjin Wang[1], Hai Cheng[2,3], R. L. Edwards[3], Xinggong Kong[1], Shitao Chen[1], and Shushuang Liu[1]**

[1]College of Geography Science, Nanjing Normal University, Nanjing, China, [2]Institute of Global Environmental Change, Xi'an Jiaotong University, Xi'an, China, [3]Department of Geology and Geophysics, University of Minnesota, Minneapolis MN, USA

**Abstract** Detailed Asian summer monsoon (ASM) variability across Heinrich stadials (HSs) 5 to 2 was reconstructed from four stalagmite oxygen isotopic ($\delta^{18}O$) records in central and southern China. For the last glacial period, these speleothem records, combined with previous cave records, reveal a rapid ASM decline at the onset of each HS. During this time, ASM intensity decreases immediately to the weakest level within approximately 50 years, which is followed by a gradual intensification in the mid-HS. Typically, this process of ASM weakening is synchronous with peak ice-rafted debris deposition and large freshwater outbursts into the North Atlantic, implying a tight link between the two. During the Holocene, however, a relatively gradual ASM decrease occurred at the start of the Bond events. Comparatively, the ASM decrease during the Bond events is generally accomplished within 110 years, and the weakest ASM occurs near the end. This difference implicates a further southward displacement of the Intertropical Convergence Zone and a stronger impact from the Atlantic meridional overturning circulation on the ASM in the early HS. Moreover, contrasting expressions of the ASM during HSs and Bond events suggest that a fixed phase relationship during bipolar climate changes cannot be expected.

**Plain Language Summary** The anatomy of internal structures in abrupt climate events under different climate boundaries is important for understanding the physical mechanisms. The $\delta^{18}O$ records from Chinese cave deposits can be used as an indicator for Asian summer monsoon (ASM) variability, which is closely related to changes of North Atlantic climates and shifts of the Intertropical Convergence Zone. In this study, a comparison of $\delta^{18}O$ records from different caves in China revealed that the ASM declined rapidly at the onset of the Heinrich events in the last glacial period but gradually at the onset of Bond events in the Holocene. This indicates that the volume of freshwater inputs into the North Atlantic during the Heinrich events was large, and the southerly movement of the Intertropical Convergence Zone was exceptionally significant. As an atmospheric bridge linking bipolar climate changes, different expressions in ASM variations in the last glacial and the Holocene should be considered when correlating northern and southern hemispheric climate changes.

## 1. Introduction

The anatomy of internal structures in abrupt climate changes is important for understanding the forcing mechanisms behind these changes. Recently, the frequency, amplitude, and duration of millennial-scale climate oscillations were suggested to be dependent on Earth's average background conditions during the last glacial period (Arzel et al., 2012; Prange et al., 2004; Romanova et al., 2004; Sima et al., 2004; Wang et al., 2008; Wang & Mysak, 2006). However, the connection between the internal structure of these climate instabilities and the mean climate state remains unclear. During Heinrich stadials (HSs), Greenland temperature frequently remains in a cold, stable phase, while higher variability can be observed in low latitudes (Corrège et al., 2004; Felis et al., 2012) and southern climates (Landais et al., 2015), reflecting a pronounced spatial diversity between them.

In the Holocene, climate instabilities (termed as Bond events) over a cycle of 1,500 years were pervasive according to terrestrial and oceanic records (Gupta et al., 2005; Wang et al., 2005). These climate variations were smaller in amplitude and shorter in duration than those of the last glacial period and had different forcing mechanisms related to contrasting background conditions. A multiproxy study on a Greenland ice

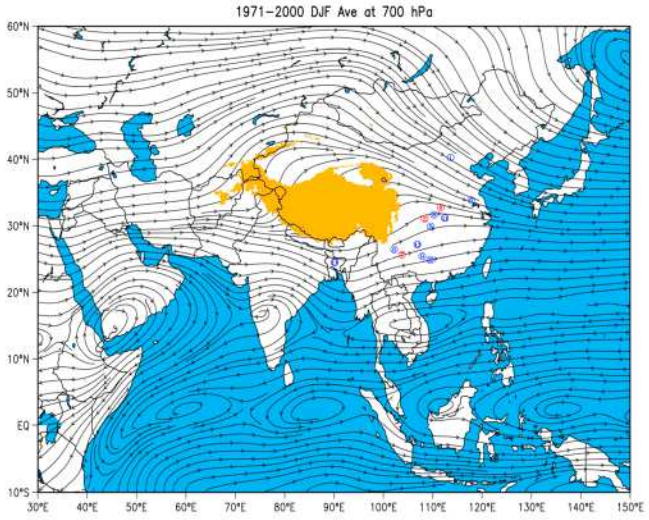


**Figure 1.** Studied locations and general circulation patterns of the Asian summer monsoon from 1971 to 2000 (NCAR/NCEP; Kalnay et al., 1996). The yellow area represents the Qinghai-Tibetan Plateau. The numbers indicate locations for the (1) Kulishu (39°41′N, 115°39′E, Ma et al., 2012), (2) Qingtian (31°20′N, 110°22′E, this study), (3) Sanbao (31°40′N, 110°26′E, Zhao et al., 2010), (4) Tian'e (31°43′N, 110°38′E, this study), (5) Heshang (30°27′N, 110°25′E, Liu, Henderson, et al., 2013), (6) Hulu (32°30′N, 119°10′E, Wang et al., 2001), (7) Wulu (26°03′N, 105°05′E, this study), (8) Dashibao (26°05′N, 105°03′E, Zhao et al., 2010), (9) Yamen (25°29′N, 107°54′E, Yang et al., 2010), (10) Dongge (25°17′N, 108°05′E, Zhao et al., 2015), (11) Yongxing (31°35′N, 111°14′E, Chen et al., 2016), (12) Qixing (25°59′N,107°16′E, Zhang et al., 2017), and (13) Mawmluh (25°15′44″N, 91°52′54″E, Berkelhammer et al., 2012) caves. These records were chosen for their high-resolution data, well-constrained chronologies, and sufficient coverage of the weak ASM events. The red numbers show cave sites where stalagmites were collected in this study. Detailed descriptions of these cave sites, locations, and local environments are listed in Table S1.

core showed that the climate anomaly surrounding 8.2 thousand years before present (ka B.P.) was approximately half the amplitude of the Younger Dryas (YD) event (Alley et al., 1997), with a more gradual temperature decline at the onset of the YD (Broecker et al., 2010). In the Asian summer monsoon (ASM) domain, the 8.2 ka climate anomaly observed in the Oman speleothem record was strikingly different from the Greenland temperature change (i.e., a gradual onset but faster end) (Fleitmann et al., 2003). Hence, these spatiotemporal discrepancies indicate that the internal structure of typical climate events is important for detecting their regional expressions or specific responses. Modeling and theoretical studies have revealed that low-latitude climate responses are composed of fast and slow components (i.e., changes in ocean overturning in the North Atlantic versus tropical oceans) (Cvijanovic & Chiang, 2013; Rohling et al., 2009). Here four high-resolution speleothem-based ASM records were reconstructed from three caves in central and southern China, separately covering HSs 5 through 2. Combined with previous cave records, we can make a detailed comparison of HSs in the last glacial period, as well as for Bond events in the Holocene.

## 2. Sites, Samples, and Methods

Four newly retrieved stalagmites were collected from three caves in China (red numbers in Figure 1). Qingtian Cave (31°20′N, 110°22′E, 1,630 m above sea level, asl) is approximately 30 km southwest of the Tian'e site (31°43′N, 110°38′E, 1,600 m asl). Both caves are located on Mount Shennongjia in central China. Qingtian Cave is approximately 50 m long and overlain by 60 to 100 m of Permian limestone bedrock. The relative humidity inside is close to 100%. The average annual surface temperature at this site is approximately 7.4°C, reaching a maximum in July (22°C) and a minimum in January (1.5°C). Mean annual precipitation ranges between 1,500 mm and 2,000 mm, approximately 80% of which falls between June and September, when the ASM prevails. Tian'e Cave is less than 80 m in length and is covered by approximately 50 m of Simian dolomite bedrock. The annual mean temperature at the nearest meteorological station (Songbai, 922 m asl) is approximately 12°C, higher in July (23.1°C) and lower in January (0.2°C). The average annual rainfall is approximately 950 mm, reaching a maximum (600 mm) between June and September and a minimum (50 mm) between December and February.

Wulu Cave (26°03´N, 105°05′E, 1,440 m asl) is 830 km southwest of the Qingtian site and is located on the Yun-Gui Plateau in southern China. The cave is approximately 800 m long, overlain by 40 m of Triassic limestone bedrock. The mean annual temperature is approximately 14°C, with a maximum in July (20.8°C) and a minimum in January (4.3°C). The annual precipitation is approximately 1,400 mm, peaking (900 mm) during summer (June through September) and reaching a minimum (80 mm) in winter (December through February).

For comparison, 10 other speleothem records were also included in this study. These studied sites cover a latitudinal range from 25°N to 39°N and a longitudinal band from 91°E to 119°E. Detailed descriptions of these speleothems can be found in the supporting information. The whole region is climatically dictated by the ASM, which is characterized by a warm/humid summer and a cold/dry winter, and 60% to 80% of the total annual precipitation occurs in the summer (June to September).

Sample QT1 was collected from the Qingtian Cave and is 492 mm in length. Stalagmites Sw4 and Sw5 are 508 and 710 mm long, respectively, and both are from Tian'e Cave. Among these samples, QT1 and Sw4 cover HS 2, and Sw5 spans HS 3. Wu30 is from the Wulu Cave in southern China and is 560 mm long. It grew during a period from HS 5 to HS 4 (Table 1). In each HS, clay bands are seldom observed on these stalagmites, indicating a continuous deposition history (see supporting information).

When halved and polished, 32 subsamples for $^{230}$Th dating were collected with a 0.9 mm diameter hand-held carbide dental drill. Measurements were performed with a Finnigan ELEMENT inductively coupled plasma

**Table 1**
*$^{230}$Th Dating Results of Four Stalagmites From Central and Southern China*

| Sample number | Depth (mm) | $^{238}$U (ppb) | $^{232}$Th (ppt) | $\delta^{234}$U (measured) | $^{230}$Th/$^{238}$U (activity) | $^{230}$Th age (yr) (uncorrected) | $^{230}$Th age (yr) (corrected) | $\delta^{234}U_{Initial}$ (corrected) |
|---|---|---|---|---|---|---|---|---|
| QT1-19 | 19 | 1,667.9 ± 3 | 2,790.8 ± 4 | 134.7 ± 2 | 0.2117 ± 0.0009 | 22,454 ± 113 | **22,412 ± 115** | 143.6 ± 2 |
| QT1-128 | 128 | 1,054.6 ± 2.7 | 777 ± 7 | 142.0 ± 2.5 | 0.2207 ± 0.0011 | 23,297 ± 140 | **23,278 ± 140** | 151.6 ± 2.6 |
| QT1-150 | 150 | 1,513.8 ± 4.7 | 462 ± 3 | 152.2 ± 2.6 | 0.2245 ± 0.0010 | 23,496 ± 128 | **23,488 ± 128** | 162.6 ± 2.8 |
| QT1-192 | 192 | 2,001.3 ± 5.6 | 813 ± 4 | 101.9 ± 2.1 | 0.2208 ± 0.0009 | 24,284 ± 126 | **24,273 ± 126** | 109.1 ± 2.2 |
| QT1-215 | 215 | 1,167.4 ± 1.4 | 935 ± 12 | 135.9 ± 1.6 | 0.2395 ± 0.0009 | 25,695 ± 115 | **25,675 ± 116** | 146 ± 2 |
| QT1-240 | 240 | 1,758 ± 2 | 562 ± 11 | 160.3 ± 1.4 | 0.2491 ± 0.0004 | 26,210 ± 62 | **26,137 ± 63** | 173 ± 2 |
| QT1-320 | 320 | 1,450.1 ± 2.3 | 828 ± 11 | 156.8 ± 2.1 | 0.25008 ± 0.0010 | 26,503 ± 129 | **26,489 ± 129** | 169 ± 2 |
| QT1-400 | 400 | 1,366 ± 1 | 772 ± 16 | 157.0 ± 1.2 | 0.2596 ± 0.0003 | 27,545 ± 53 | **27,466 ± 54** | 170 ± 1 |
| QT1-471 | 471 | 929.9 ± 2 | 2,270.9 ± 63 | 73.7 ± 2 | 0.2490 ± 0.0015 | 28,724 ± 216 | **28,659 ± 219** | 79.9 ± 3 |
| Sw4-25 | 25 | 326.4 ± 0.9 | 396.9 ± 68.5 | 170.6 ± 3.9 | 0.2151 ± 0.0028 | 22,063 ± 322 | **22,033 ± 322** | 181.6 ± 4.2 |
| Sw4-40 | 40 | 276.9 ± 0.4 | 1,090 ± 13 | 166.3 ± 1.8 | 0.2166 ± 0.0014 | 22,320 ± 160 | **22,230 ± 170** | 177.1 ± 1.9 |
| Sw4-141 | 141 | 310.9 ± 0.8 | 88.1 ± 66.9 | 167.2 ± 3.4 | 0.2178 ± 0.0023 | 22,439 ± 271 | **22,432 ± 271** | 178.2 ± 3.6 |
| Sw4-181 | 181 | 299.9 ± 1.0 | 130.2 ± 86.3 | 165.3 ± 6.2 | 0.2200 ± 0.0029 | 22,739 ± 354 | **22,728 ± 354** | 176.2 ± 6.6 |
| Sw4-200 | 200 | 330.8 ± 0.9 | 477.2 ± 68.2 | 162.4 ± 3.5 | 0.2233 ± 0.0022 | 23,173 ± 267 | **23,137 ± 268** | 173.3 ± 3.7 |
| Sw4-230 | 230 | 277.1 ± 0.4 | 2,970.0 ± 16 | 162.0 ± 1.9 | 0.2286 ± 0.0014 | 23,790 ± 170 | **23,530 ± 220** | 173.2 ± 2.1 |
| Sw4-280 | 280 | 257.5 ± 0.7 | 44.1 ± 76.5 | 156.5 ± 4.4 | 0.2280 ± 0.0027 | 23,858 ± 336 | **23,854 ± 336** | 167.5 ± 4.7 |
| Sw4-342 | 342 | 190.3 ± 0.5 | 164.1 ± 78.7 | 149.5 ± 4.7 | 0.2361 ± 0.0036 | 24,974 ± 440 | **24,952 ± 440** | 160.4 ± 5.0 |
| Sw4-400 | 400 | 171.1 ± 0.2 | 2,390 ± 12 | 151.2 ± 2.0 | 0.2456 ± 0.0016 | 26,060 ± 200 | **25,710 ± 270** | 162.5 ± 2.1 |
| Sw4-438 | 438 | 191.5 ± 0.6 | 90.7 ± 67.7 | 145.8 ± 5.0 | 0.2515 ± 0.0033 | 26,911 ± 427 | **26,899 ± 427** | 157.4 ± 5.4 |
| Sw4-467 | 467 | 183.9 ± 0.5 | 187.9 ± 64.2 | 153.5 ± 4.5 | 0.2550 ± 0.0036 | 27,126 ± 453 | **27,100 ± 453** | 165.7 ± 4.8 |
| Sw5-55 | 55 | 187.4 ± 0.4 | 10,357.7 ± 33.4 | 147.2 ± 2.7 | 0.2599 ± 0.0030 | 27,897 ± 379 | **26,500 ± 794** | 158.7 ± 3 |
| Sw5-120 | 120 | 149 ± 0 | 6,553 ± 131 | 100 ± 2 | 0.2677 ± 0.0008 | 28,602 ± 109 | **27,431 ± 790** | 154.3 ± 1.2 |
| Sw5-234 | 234 | 197.2 ± 0.4 | 3,436.8 ± 14.6 | 136.0 ± 2.6 | 0.2933 ± 0.0023 | 32,409 ± 311 | **31,967 ± 381** | 148.9 ± 2.8 |
| Sw5-420 | 420 | 160 ± 0 | 588 ± 12 | 1,366 ± 28 | 0.3051 ± 0.0009 | 33,826 ± 119 | **33,668 ± 136** | 137.5 ± 1.2 |
| Sw5-511 | 511 | 249.9 ± 0.5 | 2,366.1 ± 14.2 | 143.2 ± 2.3 | 0.3342 ± 0.0021 | 37,474 ± 296 | **37,237 ± 318** | 159.1 ± 2.5 |
| Sw5-707 | 707 | 229.6 ± 0.5 | 428.9 ± 17.8 | 133.2 ± 3.2 | 0.3411 ± 0.0024 | 38,808 ± 349 | **38,761 ± 349** | 148.6 ± 3.6 |
| Wu30-10 | 10 | 3,947 ± 7 | 1,109 ± 4 | 809.5 ± 2.9 | 0.4925 ± 0.0015 | 33,856 ± 137 | **33,852 ± 137** | 890.8 ± 3.2 |
| Wu30-112 | 112 | 2,972 ± 12 | 212 ± 6 | 788.8 ± 5.3 | 0.5261 ± 0.0026 | 36,951 ± 251 | **36,950 ± 251** | 875.6 ± 5.9 |
| Wu30-200 | 200 | 4,024 ± 5 | 750 ± 15 | 818.9 ± 2.0 | 0.5643 ± 0.0008 | 39,341 ± 85 | **39,273 ± 85** | 915 ± 2 |
| Wu30-300 | 300 | 2,946 ± 3 | 676 ± 14 | 728.4 ± 2.1 | 0.5776 ± 0.0008 | 41,444 ± 90 | **41,376 ± 90** | 879 ± 2 |
| Wu30-450 | 450 | 3,427 ± 3 | 606 ± 12 | 758.8 ± 1.9 | 0.6116 ± 0.0008 | 45,096 ± 91 | **45,028 ± 91** | 862 ± 2 |
| Wu30-556 | 556 | 4,119 ± 8 | 615 ± 3 | 769.6 ± 3.3 | 0.6751 ± 0.0019 | 50,523 ± 213 | **50,521 ± 213** | 887.7 ± 3.8 |

*Note*. Errors are 2$\sigma$ analytical errors. Decay constant values are $\lambda_{230} = 9.1577 \times 10^{-6}\ yr^{-1}$, $\lambda_{234} = 2.8263 \times 10^{-6}\ yr^{-1}$, and $\lambda_{238} = 1.55125 \times 10^{-10}\ yr^{-1}$. Corrected $^{230}$Th ages assume an initial $^{230}$Th/$^{232}$Th atomic ratio of $(4.4 \pm 2.2) \times 10^{-6}$. Corrected $^{230}$Th ages are indicated in bold and presented in years before 1,950 A.D.

mass spectrometer at the Department of Geology and Geophysics at the University of Minnesota, USA. The procedures were described in Shen et al. (2002), and results are listed in Table 1. Dating results are in stratigraphic order with typical analytical errors (2$\sigma$) varying from 50 to 790 years. Approximately 1,965 subsamples were collected for stable isotopic analysis. Sampling resolution varied from 1 to 2 mm, depending on the growth rates of the samples. Over periods covering the HS, a spacing resolution of 0.5 mm was achieved, which corresponded to a temporal resolution of 4 to 26 years. Analyses were performed on an online automated carbonate preparation system (KIEL CARBONATE DEVICE) linked to the Finnigan MAT-253 mass spectrometer at the College of Geographical Science at Nanjing Normal University. Powdered calcite samples from 50 to 80 μg were dissolved in 100% $H_3PO_4$ at 70°C. $CO_2$ was extracted from the resultant gas by cooling it to −170°C, then warming it to 30°C. Isotopic compositions were subsequently automatically measured. Standards were run every 10 to 15 samples, and duplicates were run every 15 to 20 samples to check for homogeneity. The results were reported relative to Vienna Peedee belemnite, with standardization determined relative to NBS 19. The precision of $\delta^{18}O$ values was 0.06‰ at the 1-sigma level.

## 3. Results

### 3.1. Chronology

Thirty-two $^{230}$Th dates revealed that the growth of these stalagmites separately spanned HS 5 through 2 (Table 1). The ages from isotopic data were reconstructed by an algorithm approach, MOD-AGE

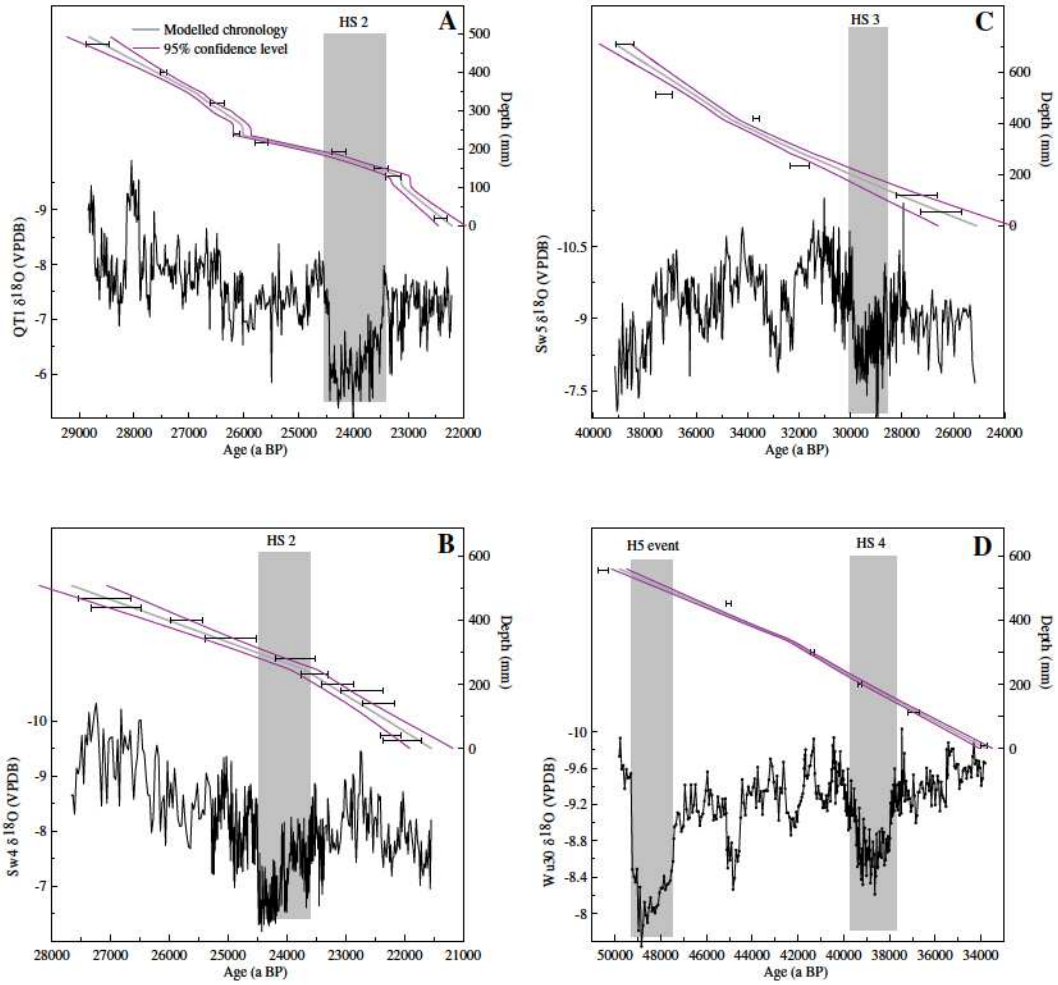


**Figure 2.** Chronologies and $\delta^{18}O$ profiles for each stalagmite from the (a) Qingtian and (b and c) Tian'e caves in central China and the (d) Wulu Cave in southern China. The HS event is labeled with gray bars. In these stalagmites, age models for $\delta^{18}O$ records were based on the MOD-AGE (gray lines), which uses a locally weighted scatterplot smoothing method (Hercman & Pawlak, 2012). The purple lines depict the 95% confidence level. Dating errors were indicated in each panel.

(Figure 2), which uses a locally weighted scatterplot smoothing method (Hercman & Pawlak, 2012). In this model, minimum assumptions are used about the age probability distributions, and it works well with irregularly sampled data. However, hiatuses in this model are expressed as a slowdown in the growth rate rather than a complete growth cessation. Four options for an age-depth model were utilized, depending on input parameters. In our modeling, normal distributions for age and depth are assumed, and the number of Monte Carlo (MC) simulations was set to 2,000. Similarly, an MC simulation was adopted to estimate confidence levels. As a result, the modeled ages generally agreed within the 95% confidence level, with linearly interpolated chronologies between adjacent $^{230}Th$ ages.

Among these samples, Sw5 has larger $^{232}Th$ values and dating errors (Table 1), and three dates from this stalagmite fall outside the envelope of modeled uncertainties (Figure 2c). Most likely, short-term growth discontinuities were present and/or large dating errors were involved. Similarly, a date from Sample Wu30 (450 mm at 45.03 ± 0.09 ka B.P.) is significantly younger than the modeled result (Figure 2d). However, other dates from this sample are generally within the confidence level of the model. In these samples, few inclusion-rich bands are observed during HSs, suggesting stable growth (see supporting information). Moreover, the age-depth relations we adopted, especially the onset timing of each HS, agreed well with other cave records from China (see supporting information), which supports the robustness of our modeled results.

### 3.2. Stalagmite Isotopic Records

Stalagmite $\delta^{18}O$ values increase by 1.5‰ to 2‰ surrounding 49, 39, 29, and 24.5 ka B.P. (Figure 2), representing a significant change in regional climates. These periods of high $\delta^{18}O$ values correspond to HSs 5 through 2. In Figure 2c, higher $\delta^{18}O$ values, which increased by 1.5‰, are also observed at approximately 33 ka B.P. in Sample Sw5, which was previously registered by the Wulu cave record (see supporting information) (Duan et al., 2014). Nevertheless, it is not comparable in magnitude to HS 3 (2‰, gray bar in Figure 2c). Thus, it is not classified as a Heinrich stadial. During each HS, maximum $\delta^{18}O$ values consistently occurred in early stages, indicating that climate conditions jumped directly and rapidly to extreme levels at the onset. The most striking characteristic for these speleothem-based HSs is an asymmetric "V" shape in the $\delta^{18}O$ profiles, that is, a sharp and significant enrichment in $\delta^{18}O$ values at the onset (into the HS), a gradual $\delta^{18}O$ depletion in the mid-HS, and a rapid jump to negative $\delta^{18}O$ values at the end (out of the HS). This feature of $\delta^{18}O$ variability has been pervasively observed in previous speleothem records from the ASM area (see supporting information) (Chen et al., 2016; Duan et al., 2014; Wang et al., 2001; Zhang et al., 2014; Zhao et al., 2010).

Along the growth axes, correlation coefficients between $\delta^{18}O$ and $\delta^{13}C$ for the newly retrieved stalagmites are small ($r^2$ = 0.01–0.11) and generally less than 0.1 (see supporting information), suggesting that they were deposited close to isotopic equilibrium with the infiltration water (Hendy, 1971). Moreover, the growth rate in the early HS exhibits little variability when $\delta^{18}O$ values increase, indicating that growth dynamics are not responsible for isotopic changes. Rapid $\delta^{18}O$ variability during the early HS and general $\delta^{18}O$ depletion in the mid-HS are equally well reflected in the spatially separated cave records from China (see supporting information). This strong duplication shows that they are of the same climatic origin (Dorale & Liu, 2009).

Mean values and standard deviations (SDs) for these $\delta^{18}O$ records were calculated (Figures 3g–3j). Following Thomas et al. (2007), the limits of HSs are defined by depths where the isotopic values fall consistently more than the mean. Thomas et al. (2007) calculated the mean and SD using 1,000 year long periods of data before and after the event. This method works well in diagnosing the climate anomaly. However, our speleothem records have different time spans and sampling resolutions. For consistency, we calculated the mean and SD for the total time series to avoid various criteria being chosen. Generally, $\delta^{18}O$ increases to its maximum value within less than 200 years during the early HS depending on growth rate and data resolution, which is less than 0.5% of the total event duration on average (Figures 3g–3j and Table 2). This $\delta^{18}O$ shift was mainly accomplished within decades (a 1‰ to 1.5‰ increase in approximately 50 years), which is broadly close to a $\delta^{18}O$ enrichment of 0.4‰ within 10 years.

During HS 4, an initial $\delta^{18}O$ increase from 620 to 960 years can be seen in samples Wu30 and YX51 (Chen et al., 2016) (Figure 3j and Table 2), which is significantly longer than during other HSs (Figures 3g–3i). Currently, the impact of regional climates on HS 4 cannot be decisively excluded. However, a banded stalagmite from the Yongxing Cave in central China shows that the start of HS 4 was accomplished within 44 years. Thus, either dating uncertainties, data resolution, or sample-specific processes were probably involved.

## 4. Discussion

### 4.1. Climatic Interpretation of Speleothem $\delta^{18}O$ Records From the ASM Area

In previous studies, the precipitation amount was believed to not be valid enough to interpret changes in cave $\delta^{18}O$ records from China (Dayem et al., 2010; Lee et al., 2009; Maher, 2008; Maher & Thompson, 2012). Especially, modern monsoonal rainfall exhibited an inferred correlation scale length of less than 500 km (Dayem et al., 2010). This was inconsistent with the coherence of speleothem $\delta^{18}O$ records over a wide range of regions. Thus, vapor sources, moisture routes, and in-cave processes were probably involved (Fairchild et al., 2006; Lachniet, 2009; Maher & Thompson, 2012; McDermott, 2004; Tan, 2014). Indeed, the speleothem $\delta^{18}O$ signal can trace changes in isotopic precipitation compositions, which can display spatial coherence over distant sites (Vuille et al., 2005) but not rainfall amounts. In the ASM area, more $^{18}O$-depleted rainfall (over 55% of the annual total) occurs in summer (June to September) (Wang & Ding, 2008). Seasonal differences between summer and winter precipitation $\delta^{18}O$ can reach 5‰ in eastern China, which is where most cave sites in Figure 1 are located (Araguás-Araguás et al., 1998). Consequently, the ASM circulation is important for moisture transfer and precipitation $\delta^{18}O$ variability, which is subsequently inherited by stalagmites deposited in the cave.

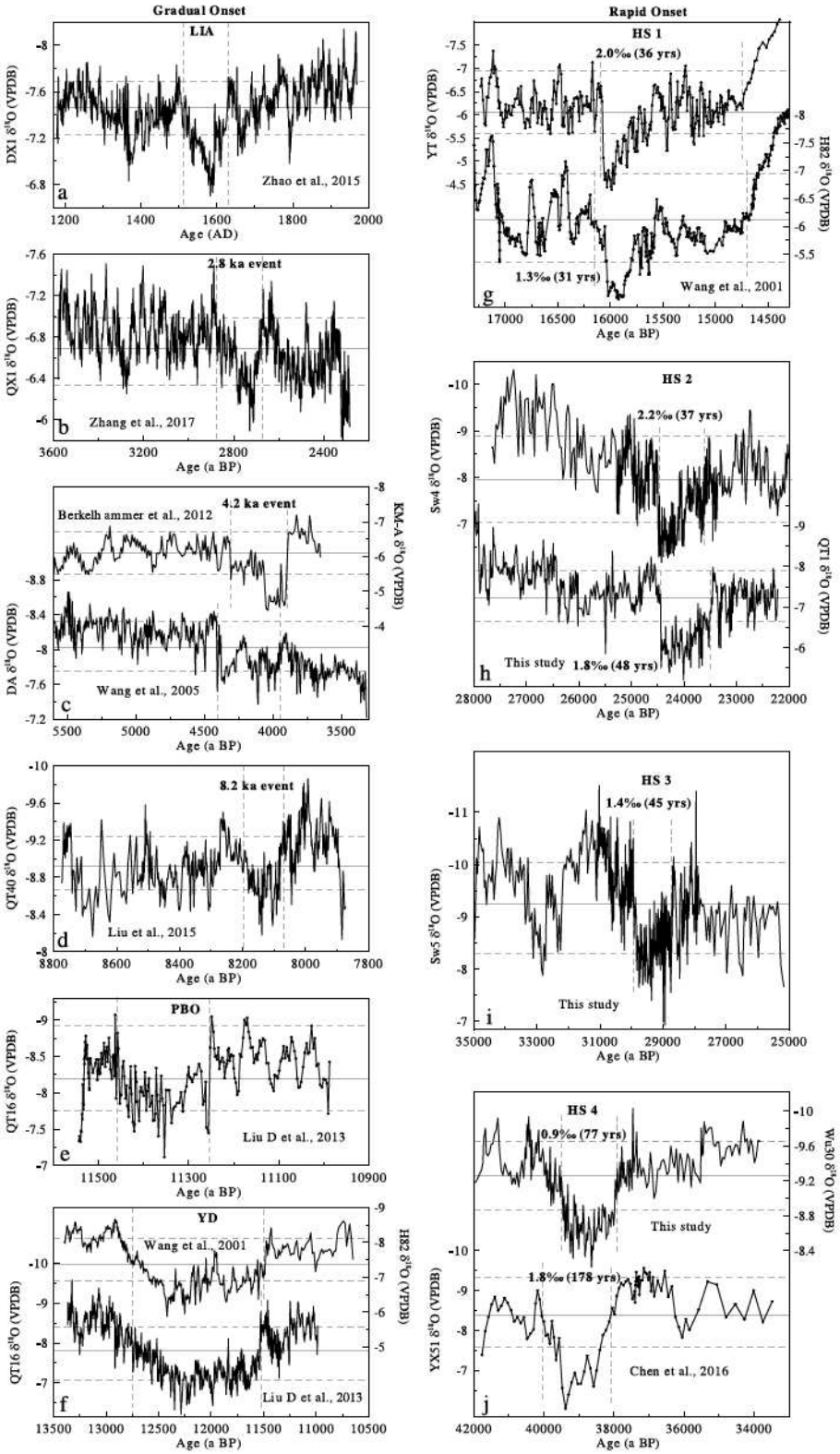


**Figure 3.** Determination of the onset, termination, and duration of climate anomalies. Procedures refer to Thomas et al. (2007). The solid gray lines in these speleothem records show average values, the horizontal dashed lines indicate one standard deviation, and the vertical dashed lines depict the onset and termination of these events. (right column) The numbers label the timing and amplitude of major processes in initial and abrupt transitions. Data sources are similar to those in Figure S3.

**Table 2**
*The Timing and Internal Structure of Chosen Weak ASM Events*

| Event type | Events | Samples | Onset timing | End timing | Assumed "zero" age[a] | Duration of initial ASM decline and its portion of the total event[b] | Changing rate of initial AM decline | References |
|---|---|---|---|---|---|---|---|---|
| Gradual onset | LIA (central event) | DX1 (Dongge Cave, Southern China) | 1,500 A.D. | 1,629 A.D. | 1,589 A.D. | 89 years (69%) | 0.11‰/10 years | (Zhao et al., 2015) |
| | 2.8 kyr event | QX1 (Qixing Cave, Southern China) | 2,879 a B.P. | 2,667 a B.P. | 2,713 a B.P. | 166 years (78%) | 0.09‰/10 years | (Zhang et al., 2016) |
| | 4.2 kyr event | KM-A (Mawmluh Cave, NE Indian) | 4,313 a B.P. | 3,887 a B.P. | 4,037 a B.P. | 276 years (65%) | 0.08‰/10 years | (Berkelhammer et al., 2012) |
| | | DA (Dongge Cave, Southern China) | 4,418 a B.P. | 3,951 a B.P. | 4,354 a B.P. | 64 years (14%) | 0.13‰/10 years | (Wang et al., 2005) |
| | 8.2 kyr event | QT40 (Qingtian Cave, central China) | 8,258 a B.P. | 8,071 a B.P. | 8,139 a B.P. | 119 years (64%) | 0.11‰/10 years | (Liu et al., 2015) |
| | PBO | QT16 (Qingtian Cave, central China) | 11,463 a B.P. | 11,252 a B.P. | 11,354 a B.P. | 109 years (52%) | 0.18‰/10 years | (Liu, Wang, et al., 2013) |
| | YD | H82 (Hulu Cave, Eastern China) | 12,864 a B.P. | 11,442 a B.P. | 12,421 a B.P. | 443 years (31%) | 0.05‰/10 years | (Wang et al., 2001) |
| | | QT16 (Qingtian Cave, central China) | 12,860 a B.P. | 11,540 a B.P. | 12,287 a B.P. | 573 years (43%) | 0.04‰/10 years | (Liu, Wang, et al., 2013) |
| Abrupt onset | Hs 1 | YT (Hulu Cave, Eastern China) | 16,078 a B.P. | 14,689 a B.P. | 16,032 a B.P. | 46 years (0.03%) | 0.46‰/10 years | (Wang et al., 2001) |
| | | H82 (Hulu Cave, Eastern China) | 16,182 a B.P. | 14,609 a B.P. | 16,021 a B.P. | 161 years (0.10%) | 0.40‰/10 years | (Wang et al., 2001) |
| | Hs 2 | Sw4 (Tian'e Cave, central China) | 24,593 a B.P. | 23,530 a B.P. | 24,480 a B.P. | 113 years (0.11%) | 0.43‰/10 years | This Study |
| | | QT1 (Qingtian Cave, central China) | 24,546 a B.P. | 23,448 a B.P. | 24,432 a B.P. | 114 years (0.10%) | 0.42‰/10 years | This Study |
| | Hs 3 | Sw5 (Tian'e Cave, central China) | 29,944 a B.P. | 28,691 a B.P. | 29,759 a B.P. | 185 years (0.15%) | 0.22‰/10 years | This Study |
| | Hs 4 | YX51 (Yongxing Cave, central China) | 40,002 a B.P. | 37,855 a B.P. | 39,385 a B.P. | 617 years (0.29%) | 0.04‰/10 years | (Chen et al., 2016) |
| | | Wu30 (Wulu Cave, Southern China) | 40,127 a B.P. | 37,904 a B.P. | 39,163 a B.P. | 964 years (0.43%) | 0.02‰/10 years | This Study |

[a]The "zero" age was designated by maximum $\delta^{18}O$ values in the early part of these events, when the ASM reached its weakest level. [b]The portion of the initial ASM decline relative to the event length was estimated by a ratio of (onset timing-zero age)/(onset timing-end timing).

In the Holocene, the long-term evolution of Chinese speleothem $\delta^{18}O$ records has been supported by annually averaged simulated precipitation $\delta^{18}O$ changes (LeGrande & Schmidt, 2009) and follows changes in synthesized lake authigenic carbonate $\delta^{18}O$ records from monsoonal regions in China (Zhang et al., 2011); this is a proxy for lake water isotopic composition associated with monsoonal rainfall. Moreover, the low speleothem $\delta^{18}O$ values (suggesting a strong ASM) in the early Holocene match well with a period of high lake-levels in northern China (40°41′–41°43′N, 112°49′–113°40′E; Zhang et al., 2016). Apparently, these proxy indicators are all related to hydrological conditions. Hence, we believe that the speleothem $\delta^{18}O$ signal should reflect ASM changes, which is consistent with ideas presented by Maher and Thompson (2012) and Tan (2014).

### 4.2. Forcing Mechanisms of Rapid ASM Changes During HSs

For the last glacial period, climate anomalies during HSs are believed to be related to a slowdown or shutdown in the Atlantic meridional overturning circulation (AMOC), caused by freshwater discharges into the North Atlantic (Ganopolski & Ramstrf, 2001; Knutti et al., 2004). This scenario might hold true during the YD and the 8.2 ka event due to the concurrence of freshwater pulses (Ellison et al., 2006; Kleiven et al., 2008). Such climate signals of cold/arid anomalies around the North Atlantic can be transmitted into Asian interiors via atmospheric teleconnections (Porter & An, 1995).

If the AMOC disturbance acts as a trigger for the HS, the rapid ASM decline during the early HS suggests a significant reduction in the oceanic conveyor. During HS 1, two peaks in ice-rafted debris (IRD) occurred at Site U1308 within the North Atlantic (49°52.66′N, 24°14.29′W; Hodell et al., 2017) (Figure 4b), with a larger volume occurring at approximately 16.1 ka B.P. Concurrently, bulk carbonate $\delta^{18}O$ values strikingly

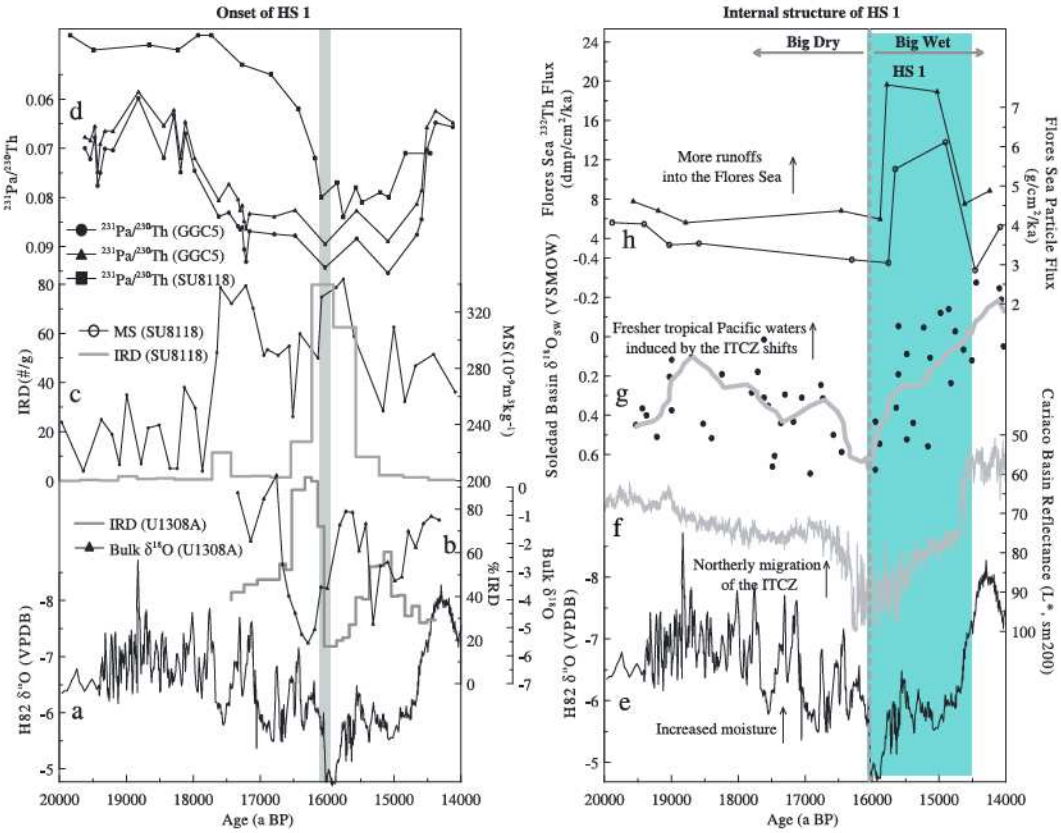


**Figure 4.** Correlations between (left) oceanic and speleothem records and (right) detailed regional climate responses surrounding HS 1. (a) H82 $\delta^{18}O$ record from Hulu Cave (Wang et al., 2001), (b) ice-rafted debris (IRD) and bulk $\delta^{18}O$ records from Site U1308A (49°52.66′N, 24°14.29′W) (Hodell et al., 2017), (c) IRD and magnetic susceptibility records from Site SU8118 in the northeast Atlantic (37°46′N, 10°11′W) (Bard et al., 2000), and (d) $^{231}Pa/^{230}Th$ records from Sites SU8118 (Gherardi et al., 2005) and GGC5 in the western subtropical Atlantic (33°42′N, 57°35′W) (McManus et al., 2004). The gray bars in this panel indicate the early HS 1. (e) The H82 $\delta^{18}O$ record from the Hulu Cave (Wang et al., 2001), (f) sediment reflectance from the Cariaco Basin (Deplazes et al., 2013), and (g) local seawater $\delta^{18}O$ changes in the Soledad Basin in the northeast Pacific (Rodríguez-Sanz et al., 2013). The black dots show scattered data, and the gray line depicts the result smoothed by a low-pass filter of 750 years; (h) $^{232}Th$ and particle fluxes from the Flores Sea in Indonesia (Muller et al., 2012). The blue bar illustrates the mid-HS 1, and the dotted line shows the "Big Dry"/"Big Wet" transition coined by Broecker and Putnam (2012).

decreased, suggesting large freshwater outputs during the early HS 1. At the Iberian Margin, a strong peak in the magnetic susceptibility record appeared older (~17.5 ka B.P.) in core SU8118 (37°46′N; 10°11′W, Bard et al., 2000) (Figure 4c). Nevertheless, the marine reservoir age of 400 years used by Bard et al. (2000) might be appreciably small, and a reservoir correction of >1,000 years would make the SU8118 age consistent with the U1308 record (Hodell et al., 2017). Furthermore, the Atlantic oceanic circulation estimated by $^{231}Pa$ and $^{230}Th$ records exhibited a significant decline during the early HS 1 (Gherardi et al., 2005; McManus et al., 2004) (Figure 4d), which was close to a total shutoff. Thus, changes in the AMOC derived from these oceanic sediments are consistent with the ASM decline at 16 ka B.P. (Wang et al., 2001) (Figure 4a), implicating a tight link between them. Dynamically, meltwaters in the North Atlantic can intrude as far south as 40°N (Hemming, 2004), inducing an expansion of the sea ice extent and lowering sea surface temperatures, thus creating a reduction in Asian moisture levels (Li et al., 2005).

In mid-HS, depleted speleothem $\delta^{18}O$ values reveal an intensification of the ASM (Figures 3g–3j). For example, during HS 1, ASM strengthening began at approximately 15.9 ka B.P., immediately after the sharp decline (dotted line in Figure 4e). This feature is similarly reflected in other HSs (Figure 3). At the Cariaco Basin, an increase in darker deposition (i.e., low reflectance values caused by more runoff) during the mid-HS 1 was nearly synchronous with Asian hydroclimatic changes (Deplazes et al., 2013) (Figure 4f). After 16 ka B.P., seawater $\delta^{18}O$ values from the Soledad Basin in the extratropical Pacific Ocean significantly decreased, indicating the presence of freshwater masses (Rodríguez-Sanz et al., 2013) (Figure 4g). In Indonesia, the concomitant enhancement of $^{232}Th$ and particle fluxes from piston core VM33-80 in the Flores Sea suggested an increase

in detrital materials from surrounding landmasses induced by northeast monsoon strengthening (Muller et al., 2012) (Figure 4h). Thus, this "16 ka transition" is likely a significant climate reorganization that is widely observed at middle to low latitudes. Temporally, it coincides with the shift from the "Big Dry" episode to the "Big Wet" episode during the mysterious interval dubbed by Broecker and Putnam (2012). Because changes in the average position of the Intertropical Convergence Zone (ITCZ) are important for low-latitude moisture transfer and availability, these observations call for a relatively northern displacement of the ITCZ in the mid-HS (Deplazes et al., 2013; Rodríguez-Sanz et al., 2013). The structures of other HSs are similar in our speleothem records; hence, high-resolution and well-dated oceanic studies are needed to test whether an analogous imprint can be found comparable to ASM records.

### 4.3. Contrasting Patterns of HSs and Bond Events

In the last 10 ka, climate instabilities (Bond events) were reported to punctuate the stable Holocene at a pace of ~1,500 yrs (Bond et al., 1997). Although these climate oscillations are not comparable to HSs in the last glacial period regarding the amplitude, duration, and remote effect, it has been suggested that AMOC variability could be involved in some cases (Bond et al., 1997; Ellison et al., 2006). The Bond events in Asian speleothem $\delta^{18}O$ records generally fall within a range of 0.8 to 1‰ (see supporting information), which is indicative of a noticeable ASM decline during these periods (Berkelhammer et al., 2012; Dykoski et al., 2005; Liu, Henderson, et al., 2013; Liu et al., 2015, 2017; Sinha et al., 2007; Zhao et al., 2015; Zhang et al., 2017). These cave records were constrained by precisely dated or annually counted chronologies that were well reproduced at a centennial scale. This provided a chance to detect the internal structures of abrupt climate changes in the Holocene.

Mean values and SDs for these Holocene $\delta^{18}O$ records were calculated (Figure 3, left column). These ASM depression events are all characterized by a gradual onset. The initial ASM decline is estimated to span 60 to 270 years, accounting for a great portion of the total event (generally over 40%) (Table 2). This is approximately equivalent to a $\delta^{18}O$ enrichment of 0.1‰ within 10 years, with about one-fourth of that occurring in early HSs. Maximum $\delta^{18}O$ values generally occur near the end of Bond events. This gradual pattern in $\delta^{18}O$ changes is also reflected at the onset of the YD (Liu, Wang, et al., 2013; Ma et al., 2012; Wang et al., 2001; Yang et al., 2010) (see supporting information and Figure 3f). Consequently, the initial $\delta^{18}O$ increase (i.e., ASM decline) spans, on average, periods of 50, 110, and over 500 years at the onset of HS, Bond, and YD events, respectively (Figure 5).

Contrasting expressions in ASM changes over HSs and Bond events are likely the result of different physical mechanisms or divergent responses under various background conditions. In the past 500 ka, repeated peaks in IRD deposition in the North Atlantic mainly occurred during glacials and deglaciations that contrast with interglacial periods (McManus et al., 1999), which indicate larger freshwater discharges during HSs than in the Holocene. Thus, a smaller volume of freshwater inputs into the North Atlantic during the Holocene should not cause a significant AMOC reduction, and a gradual decline in Asian hydrological conditions can be deduced. In response to AMOC changes, the average position of the ITCZ, controlled by heat transport between hemispheres, shifts southward by 5° to 7° in northern cold episodes (Arbuszewski et al., 2013; Sachs et al., 2009), with a larger movement in the tropical Pacific Ocean during the HS (McGee et al., 2014). Hence, more southerly movement of the ITCZ during HSs should pull primary hydrological and atmospheric activities in the Pacific Ocean significantly away from the Asian interior and further decrease the ASM intensity.

Various forcing mechanisms were invoked to interpret Bond events in the Holocene (Wanner et al., 2008, and the references therein). However, it is not assured that the combined effect of the AMOC and the ITCZ is responsible for the gradual ASM decrease at the onset of Bond events. Indeed, smaller volumes in freshwater inputs were needed to drive Holocene climate instabilities in modeling studies (Gong et al., 2013), and the southerly ITCZ shift in the Holocene was believed to cover a narrower latitudinal range (Haug et al., 2001; Sachs et al., 2009). This is likely the reason why the ASM declined so gradually during Bond events. The different structures of HS and Bond events should be addressed with caution when building a bipolar climate correlation, as the midpoint of abrupt climate transitions is often applied as a reference. Hence, at least two modes of bipolar climate correlations should be used, and a consistent lead/lag relationship between interhemispheric climates still needs to be validated, as suggested by Neukom et al. (2014) and Raisbeck et al. (2017).

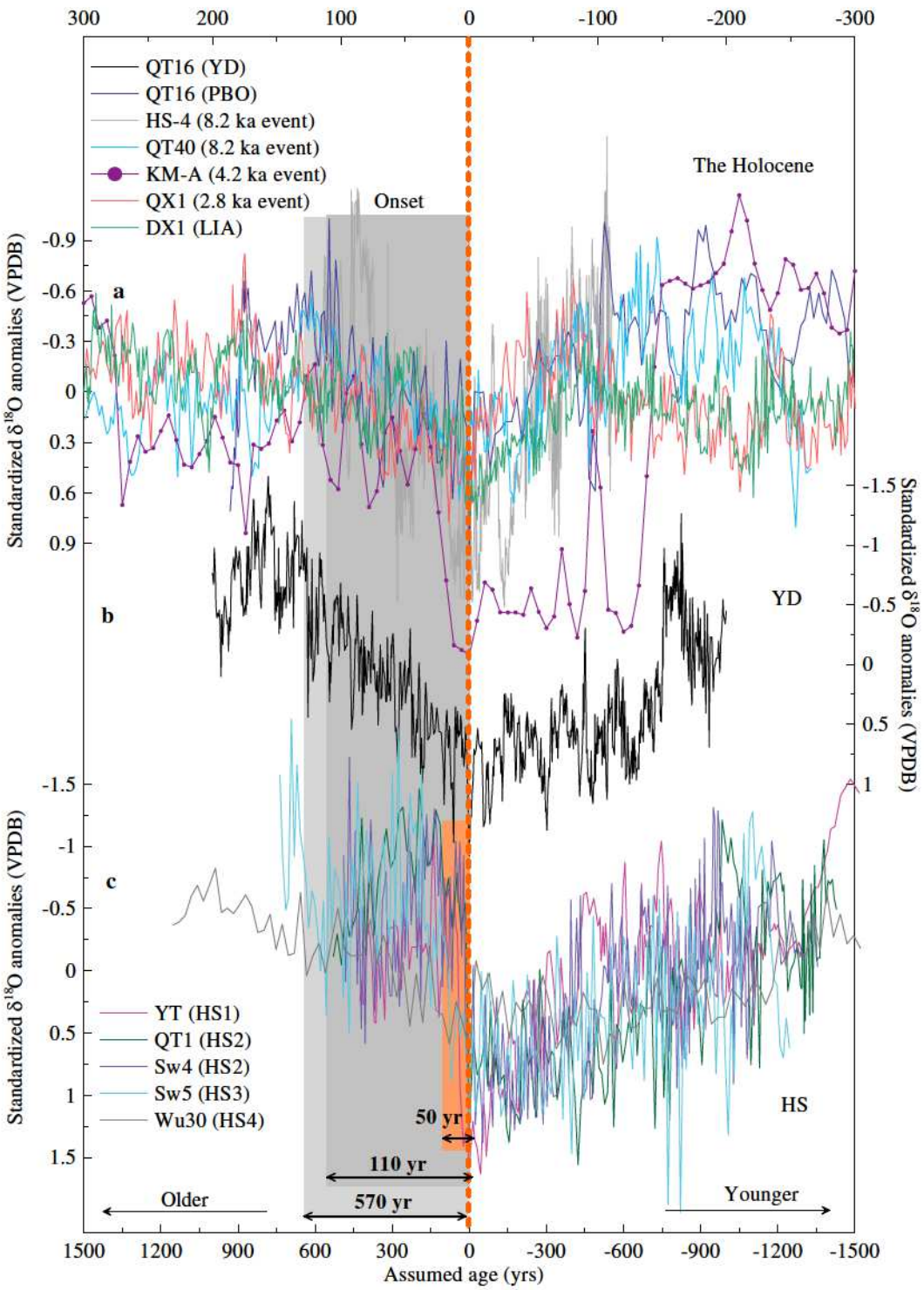


**Figure 5.** Comparison of standardized $\delta^{18}O$ records in the (a) Holocene, the (b) YD, and the (c) last glacial. These records were plotted by an assumed age, and the "zero age" (brown dashed line) was determined by maximum $\delta^{18}O$ values during these events. The YD and HSs were plotted on the bottom axis, and Holocene climate events were drawn on the top axis. The light gray bar indicates the onset of the YD, the dark gray bar indicates the onset of Bond events, and the brown bar indicates the onset of HSs.

## 5. Conclusion

Four stalagmite $\delta^{18}O$ records from three caves in central and southern China revealed detailed ASM variability that separately covered HSs 5 through 2. These speleothem-based HSs are characterized by an abrupt onset (generally within less than 200 years, and the major transition is accomplished in approximately 50 years). The weakest ASM occurred in the early HS, followed by a gradual intensification in the mid-HS. This asymmetrical "V" shape in the HS event is widely reflected in other cave records, and the initial ASM decline corresponds to a large IRD peak in the North Atlantic, indicating an impact of the AMOC on the Asian hydroclimate. Recovery of the ASM in the mid-HSs, attributed to a northerly shift in the ITCZ, is strongly represented in these low-latitude hydrological records.

When compared with Holocene speleothem records, different patterns in ASM responses can be observed. In the Holocene, centennial-scale ASM depressions (including the YD) feature a gradual onset. The initial $\delta^{18}O$ increase generally lasts 110 years, which is significantly slower than $\delta^{18}O$ variability in the early HS, and the weakest ASM is frequently positioned near the end of the Bond events. Therefore, these contrasting patterns in HSs and Bond events merit attention in future studies when correlating bipolar climate changes.

**Acknowledgments**
We are grateful to two anonymous reviewers for their generous technical comments on an early version of this manuscript. This work was jointly supported by grants from the National Key R&D Program of China (2016YFA0600401) and the National Nature Science Foundation of China (41672161, 41731174 and 1702816), a project funded by the Priority Academic Program Development (PAPD) of Jiangsu Higher Education Institutions (164320H116), the Jiangsu Center for Collaborative Innovation in Geographical Information Resource Development and Application, and the Key Laboratory of Virtual Geographic Environments (Nanjing Normal University). All data are archived with NOAA (https://www.ncdc.noaa.gov/data-access/paleoclimatology-ata) information systems.

## References

Alley, R. B., Mayewski, P. A., Sowers, T., Stuvier, M., Taylor, K. C., & Clark, P. U. (1997). Holocene climatic instability: A prominent, widespread event 8200 yr ago. *Geology*, *25*(6), 483–486. https://doi.org/10.1130/0091-7613(1997)025%3C0483:HCIAPW%3E2.3.CO;2

Araguás-Araguás, L., Froehlich, K., & Rozanski, K. (1998). Stable isotope composition of precipitation over southeast Asia. *Journal of Geophysical Research*, *103*(D22), 28,721–28,742. https://doi.org/10.1029/98JD02582

Arbuszewski, J. A., deMenocal, P. B., Cléroux, C., Bradtmiller, L., & Mix, A. (2013). Meridional shifts of the Atlantic intertropical convergence zone since the Last Glacial Maximum. *Nature Geoscience*, *6*, 1–4.

Arzel, O., Egland, M. H., de Verdière, A. C., & Huck, T. (2012). Abrupt millennial variability and interdecadal-interstadial oscillations in a global coupled model: Sensitivity to the background climate state. *Climate Dynamics*, *39*(1-2), 259–275. https://doi.org/10.1007/s00382-011-1117-y

Bard, E., Rostek, F., Turon, J.-L., & Gendreau, S. (2000). Hydrological impact of Heinrich events in the subtropical northeast Atlantic. *Science*, *289*(5483), 1321–1324. https://doi.org/10.1126/science.289.5483.1321

Berkelhammer, M., Sinha, A., Stott, L., Cheng, H., Pausata, F. S. R., & Yoshimura, K. (2012). An abrupt shift in the Indian monsoon 4000 years ago. In L. Giosan, et al. (Eds.), *Climates, landscapes, and civilizations, Geophysical Monograph* (Vol. 198, pp. 75–87). Washington, DC: American Geophysical Union.

Bond, G., Showers, W., Cheseby, M., Lotti, R., Almasi, P., deMenocal, P., … Bonani, G. (1997). A pervasive millennial-scale cycle in North Atlantic Holocene and glacial climates. *Science*, *278*(5341), 1257–1266. https://doi.org/10.1126/science.278.5341.1257

Broecker, W. S., Denton, G. H., Edwards, R. L., Cheng, H., Alley, R. B., & Putnam, A. E. (2010). Putting the Younger Dryas cold event into context. *Quaternary Science Reviews*, *29*(9-10), 1078–1081. https://doi.org/10.1016/j.quascirev.2010.02.019

Broecker, W., & Putnam, A. E. (2012). How did the hydrologic cycle respond to the two-phase mystery interval? *Quaternary Science Reviews*, *57*, 17–25. https://doi.org/10.1016/j.quascirev.2012.09.024

Chen, S. T., Wang, Y. J., Cheng, H., Edwards, R. L., Wang, X. F., Kong, X. G., & Liu, D. B. (2016). Strong coupling of Asian monsoon and Antarctic climates on sub-orbital timescales. *Scientific Reports*, *6*(1), 32995. https://doi.org/10.1038/srep32995

Corrège, T., Gagan, M. K., Beck, J. W., Burr, G. S., Cabioch, G., & Cornec, F. L. (2004). Interdecadal variation in the extent of South Pacific tropical waters during the Younger Dryas event. *Nature*, *428*(6986), 927–929. https://doi.org/10.1038/nature02506

Cvijanovic, I., & Chiang, J. H. (2013). Global energy budget changes to high latitude North Atlantic cooling and the tropical ITCZ response. *Climate Dynamics*, *40*(5-6), 1435–1452. https://doi.org/10.1007/s00382-012-1482-1

Dayem, K. E., Molnar, P., Battisti, D. S., & Roe, G. H. (2010). Lessons learned from oxygen isotopes in modern precipitation applied to interpretation of speleothem records of paleoclimate from eastern China. *Earth and Planetary Science Letters*, *295*, 219–230.

Deplazes, G., Lückge, A., Peterson, L. C., Timmermann, A., Hamann, Y., Hughen, K. A., … Haug, G. H. (2013). Links between tropical rainfall and North Atlantic climate during the last glacial period. *Nature Geoscience*, *6*(3), 213–217. https://doi.org/10.1038/ngeo1712

Dorale, J. A., & Liu, Z. H. (2009). Limitations of hendy test criteria in judging the paleoclimatic suitability of speleothems and the need for replication. *Journal of Cave and Karst Studies*, *71*, 73–80.

Duan, F. C., Liu, D. B., Cheng, H., Wang, X. F., Wang, Y. J., Kong, X. G., & Chen, S. T. (2014). A high-resolution monsoon record of millennial-scale oscillations during late MIS 3 from Wulu Cave, south-west China. *Journal of Quaternary Science*, *29*(1), 83–90. https://doi.org/10.1002/jqs.2681

Dykoski, C. A., Edwards, R. L., Cheng, H., Yuan, D. X., Cai, Y. J., Zhang, M. L., … Revenaugh, J. (2005). A high-resolution, absolute-dated Holocene and deglacial Asian monsoon record from Dongge Cave, China. *Earth and Planetary Science Letters*, *233*, 71–86.

Ellison, C. R., Chapman, M. R., & Hall, I. R. (2006). Surface and deep ocean interactions during the cold climate event 8200 years ago. *Science*, *312*(5782), 1929–1932. https://doi.org/10.1126/science.1127213

Fairchild, I. J., Smith, C. L., Baker, A., Fuller, L., Spötl, C., Mattey, D., … E. I. M. F. (2006). Modification and preservation of environmental signals in speleothems. *Earth Science Reviews*, *75*(1-4), 105–153. https://doi.org/10.1016/j.earscirev.2005.08.003

Felis, T., Merkel, U., Asami, R., Deschamps, P., Hathorne, E. C., Kölling, M., … Pfeiffer, M. (2012). Pronounced interannual variability in tropical South Pacific temperatures during Heinrich Stadial 1. *Nature Communications*, *3*, 965. https://doi.org/10.1038/ncomms1973

Fleitmann, D., Burns, S. J., Mudelsee, M., Neff, U., Kramers, J., Mangini, A., & Matter, A. (2003). Holocene forcing of the Indian monsoon recorded in a stalagmite from southern Oman. *Science*, *300*(5626), 1737–1739. https://doi.org/10.1126/science.1083130

Ganopolski, A., & Ramstrf, S. (2001). Rapid changes of glacial climate simulated in a coupled climate model. *Nature*, *409*(6817), 153–158. https://doi.org/10.1038/35051500

Gherardi, J.-M., Labeyrie, L., McManus, J. F., Francois, R., Skinner, L. C., & Cortijo, E. (2005). Evidence from the northeastern Atlantic basin for variability in the rate of meridional overturning circulation through the last deglaciation. *Earth and Planetary Science Letters*, *240*, 710–723.
Gong, X., Knorr, G., Lohmann, G., & Zhang, X. (2013). Dependence of abrupt Atlantic meridional ocean circulation changes on climate background states. *Geophysical Research Letters*, *40*, 3698–3704. https://doi.org/10.1002/grl.50701
Gupta, A. K., Das, M., & Anderseon, D. M. (2005). Solar influence on the Indian summer monsoon during the Holocene. *Geophysical Research Letters*, *32*, L17703. https://doi.org/10.1029/2005GL22685
Haug, G. H., Hughen, K. A., Sigman, D. M., Peterson, L. C., & Rühl, U. (2001). Southward migration of the Intertropical Convergence Zone through the Holocene. *Science*, *293*(5533), 1304–1308. https://doi.org/10.1126/science.1059725
Hemming, S. R. (2004). Heinrich events: Massive late Pleistocene detritus layers of the North Atlantic and their global climate imprint. *Reviews of Geophysics*, *42*, RG1005. https://doi.org/10.1029/2003RG000128
Hendy, C. H. (1971). The isotopic geochemistry of speleothems—I. The calculation of the effects of different modes of formation on the isotopic composition of speleothems and their applicability as paleoclimatic indicators. *Geochimica et Cosmochimica Acta*, *35*, 801–824.
Hercman, H., & Pawlak, J. (2012). MOD-AGE: An age-depth model construction algorithm. *Quaternary Geochronology*, *12*, 1–10. https://doi.org/10.1016/j.quageo.2012.05.003
Hodell, D. A., Nicholl, J. A. T. R. R., Bontognali, S., Danino, J., Dorador, J., Dowdeswell, A., … Röhl, U. (2017). Anatomy of Heinrich layer 1 and its role in the last deglaciation. *Paleoceanography*, *32*, 284–303. https://doi.org/10.1002/2016PA003028
Kalnay, E., Kanamitsu, M., Kistler, R., Collins, W., Deaven, D., Gandin, L., … Joseph, D. (1996). The NCEP/NCAR 40-year reanalysis project. *Bulletin of the American Meteorological Society*, *77*(3), 437–471. https://doi.org/10.1175/1520-0477(1996)077%3C0437:TNYRP%3E2.0.CO;2
Kleiven, H. F., Kissel, C., Laj, C., Ninnemann, U. S., Richter, T. O., & Cortijo, E. (2008). Reduced North Atlantic deep water coeval with the glacial Lake Agassiz freshwater outburst. *Science*, *319*(5859), 60–64. https://doi.org/10.1126/science.1148924
Knutti, R., Flückiger, J., Stocker, T. F., & Timmermann, A. (2004). Strong hemispheric coupling of glacial climate through freshwater discharge and ocean circulation. *Nature*, *430*(7002), 851–856. https://doi.org/10.1038/nature02786
Lachniet, M. S. (2009). Climatic and environmental controls on speleothem oxygen-isotope values. *Quaternary Science Reviews*, *28*(5-6), 412–432. https://doi.org/10.1016/j.quascirev.2008.10.021
Landais, A., Masson-Delmotte, V., Stenni, B., Selmo, E., Roche, D. M., Jouzel, J., … Popp, T. (2015). A review of the bipolar see-saw from synchronized and high resolution ice core water stable isotope records from Greenland and East Antarctica. *Quaternary Science Reviews*, *114*, 18–32. https://doi.org/10.1016/j.quascirev.2015.01.031
Lee, J.-E., Johnson, K., & Fuang, I. (2009). Precipitation over South America during the Last Maximum: An analysis of the "amount effect" with a water isotope-enabled general circulation model. *Journal of Geophysical Research*, *36*, L19701. https://doi.org/10.1029/2009GL039265
LeGrande, A. N., & Schmidt, G. A. (2009). Sources of Holocene variability of oxygen isotopes in paleoclimate archives. *Climate of the Past*, *5*, 441–455.
Li, C., Battisti, D. S., Schrag, D. P., & Tziperman, E. (2005). Abrupt climate shifts in Greenland due to displacements of the sea ice edge. *Geophysical Research Letters*, *32*, L19702. https://doi.org/10.1029/2005GL023492
Liu, Y.-H., Henderson, G. M., Hu, C.-Y., Mason, A. J., Charnley, N., Johnson, K. R., & Xie, S.-C. (2013). Links between the East Asian monsoon and North Atlantic climate during the 8,200 year event. *Nature Geoscience*, *6*(2), 117–120. https://doi.org/10.1038/ngeo1708
Liu, D. B., Wang, Y. J., Cheng, H., Edwards, R. L., & Kong, X. G. (2015). Cyclic changes of Asian monsoon intensity during the early mid-Holocene from annually-laminated stalagmites, central China. *Quaternary Science Reviews*, *121*, 1–10. https://doi.org/10.1016/j.quascirev.2015.05.003
Liu, D. B., Wang, Y. J., Cheng, H., Edwards, R. L., & Kong, X. G. (2017). Remote vs. local control on the Preboreal Asian hydroclimate and soil processes recorded by an annually-laminated stalagmite from Daoguan Cave, southern China. *Quaternary International*, *452*, 79–90. https://doi.org/10.1016/j.quaint.2016.09.038
Liu, D. B., Wang, Y. J., Cheng, H., Kong, X. G., & Chen, S. T. (2013). Centennial-scale Asian monsoon variability during the mid-Younger Dryas from Qingtian Cave, central China. *Quaternary Research*, *80*(02), 199–206. https://doi.org/10.1016/j.yqres.2013.06.009
Ma, Z.-B., Cheng, H., Tan, M., Edwards, R. L., Li, H.-C., You, C.-F., … Kelly, M. J. (2012). Timing and structure of the Younger Dryas event in northern China. *Quaternary Science Reviews*, *41*, 83–93. https://doi.org/10.1016/j.quascirev.2012.03.006
Maher, B. A. (2008). Holocene variability of the East Asian summer monsoon from Chinese cave records: A re-assessment. *Holocene*, *18*(6), 861–866. https://doi.org/10.1177/0959683608095569
Maher, B. A., & Thompson, R. (2012). Oxygen isotopes from Chinese caves: Records not of monsoon rainfall but of circulation regime. *Journal of Quaternary Science*, *27*(6), 615–624. https://doi.org/10.1002/jqs.2553
McDermott, F. (2004). Palaeo-climate reconstruction from stable isotope variations in speleothems: A review. *Quaternary Science Reviews*, *23*(7-8), 901–918. https://doi.org/10.1016/j.quascirev.2003.06.021
McGee, D., Donohoe, A., Marshall, J., & Ferreira, D. (2014). Changes in ITCZ location and cross-equatorial heat transport at the Last Glacial Maximum, Heinrich Stadial 1, and the mid-Holocene. *Earth and Planetary Science Letters*, *390*, 69–79.
McManus, J. F., Francois, R., Gherardi, J.-M., Keigwin, L. D., & Brown-Leger, S. (2004). Collapse and rapid resumption of Atlantic meridional circulation linked to deglacial climate changes. *Nature*, *428*(6985), 834–837. https://doi.org/10.1038/nature02494
McManus, J. F., Oppo, D. W., & Cullen, J. L. (1999). A 0.5-million-year record of millennial-scale climate variability in the North Atlantic. *Science*, *283*(5404), 971–975. https://doi.org/10.1126/science.283.5404.971
Muller, J., McManus, J. F., Oppo, D. W., & Francois, R. (2012). Strengthening of the northeast monsoon over the Flores Sea, Indonesia, at the time of Heinrich event 1. *Geology*, *40*(7), 635–638. https://doi.org/10.1130/G32878.1
Neukom, R., Gergis, J., Karoly, D. J., Wanner, H., Curran, M., Elbert, J., … Frank, D. (2014). Inter-hemispheric temperature variability over the past millennium. *Nature Climate Change*, *4*, 362–367.
Porter, S. C., & An, Z. S. (1995). Correlation between climate events in the North Atlantic and China during the last glaciation. *Nature*, *375*(6529), 305–308. https://doi.org/10.1038/375305a0
Prange, M., Lohmann, G., Romanova, V., & Butzin, M. (2004). Modelling tempo-spatial signatures of Heinrich events: Influence of the climatic background state. *Quaternary Science Reviews*, *23*(5-6), 521–527. https://doi.org/10.1016/j.quascirev.2003.11.004
Raisbeck, G. M., Cauquoin, A., Jouzel, J., Landais, A., Petit, J.-R., Lipenkov, V. Y., … Yiou, F. (2017). An improved north-south synchronization of ice core records around the 41 K beryllium 10 peak. *Climate of the Past*, *13*, 217–229.
Rodríguez-Sanz, L., Mortyn, P. G., Herguera, J. C., & Zahn, R. (2013). Hydrographic changes in the tropical and extrotropical Pacific during the last deglaciation. *Paleoceanography*, *28*, 529–538. https://doi.org/10.1002/palo.20049
Rohling, E. J., Liu, Q. S., Roberts, A. P., Stanford, J. D., Rasmussen, S. O., Langen, P. L., & Siddall, M. (2009). Controls in the East Asian monsoon during the last glacial cycle, based on comparison between Hulu Cave and polar ice-core records. *Quaternary Science Reviews*, *28*(27-28), 3291–3302. https://doi.org/10.1016/j.quascirev.2009.09.007

Romanova, V., Prange, M., & Lohmann, G. (2004). Stability of the glacial thermohaline circulation and its dependence of the background hydrological cycle. *Climate Dynamics*, *22*(5), 527–538. https://doi.org/10.1007/s00382-004-0395-z

Sachs, J. P., Sachse, D., Smittenberg, R. H., Zhang, Z., Battisti, D. S., & Golubic, S. (2009). Southward movement of the Pacific intertropical convergence zone AD 1400–1850. *Nature Geoscience*, *2*(7), 519–525. https://doi.org/10.1038/ngeo554

Shen, C.-C., Edwards, R. L., Cheng, H., Dorale, J. A., Thomas, R. B., Moran, S. B., … Edmonds, H. N. (2002). Uranium and thorium isotopic and concentration measurements by magnetic sector inductively coupled plasma mass spectrometry. *Chemical Geology*, *185*(3-4), 165–178. https://doi.org/10.1016/S0009-2541(01)00404-1

Sima, A., Paul, A., & Schulz, M. (2004). The Younger Dryas—An intrinsic feature of late Pleistocene climate change at millennial timescales. *Earth and Planetary Science Letters*, *222*, 741–750.

Sinha, A., Cannariato, K. G., Stott, L. D., Cheng, H., Edwards, R. L., Yadava, M. G., … Singh, I. B. (2007). A 900-year (600 to 1500 A.D.) record of the Indian summer monsoon precipitation from the core monsoon zone of India. *Geophysical Research Letters*, *34*, L16707. https://doi.org/10.1029/2007GL030431

Tan, M. (2014). Circulation effect: Response of precipitation $\delta^{18}O$ to the ENSO cycle in monsoon regions of China. *Climate Dynamics*, *42*(3-4), 1067–1077. https://doi.org/10.1007/s00382-013-1732-x

Thomas, E. R., Wolff, E. W., Mulvaney, R., Steffensen, J. P., Johnsen, S. J., Arrowsmith, C., … Popp, T. (2007). The 8.2 ka event from Greenland ice cores. *Quaternary Science Reviews*, *26*(1-2), 70–81. https://doi.org/10.1016/j.quascirev.2006.07.017

Vuille, M., Werner, M., Bradley, R. S., & Keimig, F. (2005). Stable isotopes in precipitation in the Asian monsoon region. *Journal of Geophysical Research*, *110*, D23108. https://doi.org/10.1029/2005JD006022

Wang, Y. J., Cheng, H., Edwards, R. L., An, Z. S., Wu, J. Y., Shen, C.-C., & Dorale, J. A. (2001). A high-resolution absolute-dated late Pleistocene monsoon record from Hulu Cave, China. *Science*, *294*(5550), 2345–2348. https://doi.org/10.1126/science.1064618

Wang, Y. J., Cheng, H., Edwards, R. L., He, Y. Q., Kong, X. G., An, Z. S., … Li, X. D. (2005). The Holocene Asian monsoon: Links to solar changes North Atlantic climates. *Science*, *308*(5723), 854–857. https://doi.org/10.1126/science.1106296

Wang, Y. J., Cheng, H., Edwards, R. L., Kong, X. G., Shao, X. H., Chen, S. T., … An, Z. S. (2008). Millennial- and orbital-scale changes in the East Asian monsoon over the past 224, 000 years. *Nature*, *451*(7182), 1090–1093. https://doi.org/10.1038/nature06692

Wang, B., & Ding, Q. H. (2008). Global monsoon: Dominant mode of annual variation in the tropics. *Dynamics of Atmospheres and Oceans*, *44*(3-4), 165–183. https://doi.org/10.1016/j.dynatmoce.2007.05.002

Wang, Z. M., & Mysak, L. A. (2006). Glacial abrupt climate changes and Dansgaard-Oeschger oscillations in a coupled climate model. *Paleoceanography*, *21*, PA2001. https://doi.org/10.1029/2005PA001238

Wanner, H., Beer, J., Bütikofer, J., Crowley, T. J., Cubasch, U., Flückiger, J., … Widmann, M. (2008). Mid- to late Holocene climate changes: An overview. *Quaternary Science Reviews*, *27*(19-20), 1791–1828. https://doi.org/10.1016/j.quascirev.2008.06.013

Yang, Y., Yuan, D. X., Cheng, H., Zhang, M. L., Qin, J. M., Lin, Y. S., … Edwards, R. L. (2010). Precise dating of abrupt shifts in the Asian monsoon during the last deglaciation based on stalagmite data from Yamen Cave, Guizhou Province. *Science China: Earth Sciences*, *53*(5), 633–641. https://doi.org/10.1007/s11430-010-0025-z

Zhang, J. W., Chen, F. H., Holmes, J. A., Li, H., Guo, X. Y., Wang, J. L., … Qiang, M. R. (2011). Holocene monsoon climate documented by oxygen and carbon isotopes from lake sediments and peat bogs in China: A review and synthesis. *Quaternary Science Reviews*, *30*(15-16), 1973–1987. https://doi.org/10.1016/j.quascirev.2011.04.023

Zhang, J. R., Tsukamoto, S., Jia, Y. L., & Frechen, M. (2016). Lake level reconstruction of Huangqihai Lake in northern China since MIS 3 based on pulsed optically stimulated luminescence dating. *Journal of Quaternary Science*, *31*(3), 225–238. https://doi.org/10.1002/jqs.2861

Zhang, Z. Q., Wang, Y. J., Liu, D. B., Cheng, H., Huang, W., Wang, Q., & Liang, Y. J. (2017). Multi-scale variability of Asian monsoon recorded in a Chinese annually-banded stalagmite during the Neoglacial period. *Quaternary International*. https://doi.org/10.1016/j.quaint.2017.08.072

Zhang, W. H., Wu, J. Y., Wang, Y., Wang, Y. J., Cheng, H., Kong, X. G., & Duan, F. C. (2014). A detailed East Asian monsoon history surrounding the 'mystery interval' derived from three Chinese speleothem records. *Quaternary Research*, *82*(01), 154–163. https://doi.org/10.1016/j.yqres.2014.01.010

Zhao, K., Wang, Y. J., Edwards, R. L., Cheng, H., & Liu, D. B. (2010). High-resolution stalagmite $\delta^{18}O$ records of Asian monsoon changes in central and southern China spanning the MIS 3/2 transition. *Earth and Planetary Science Letters*, *298*, 191–198.

Zhao, K., Wang, Y. J., Edwards, R. L., Cheng, H., Liu, D. B., & Kong, X. G. (2015). A high-resolved record of the Asian summer monsoon from Dongge Cave, China for the past 1200 years. *Quaternary Science Reviews*, *122*, 250–257. https://doi.org/10.1016/j.quascirev.2015.05.030